

Spin canting as a result of the competition between stripes and spirals in cuprates

G. Seibold,¹ R.S. Markiewicz,^{2,3} and J. Lorenzana³

¹*Institut Für Physik, BTU Cottbus, PBox 101344, 03013 Cottbus, Germany*

²*Physics Department, Northeastern University, Boston MA 02115, USA*

³*ISC-CNR and Dipartimento di Fisica, Università di Roma “La Sapienza”, P. Aldo Moro 2, 00185 Roma, Italy*

(Dated: May 25, 2022)

Based on the extended Hubbard model we calculate the energy of stripe and spiral ground states. We find that uniform spirals get favored by a large t'/t ratio but are unstable at small doping towards stripes and checkerboard textures with spin canting. The structure of these inhomogeneities also depends on t'/t and the associated spin currents may induce a small lattice distortion associated with local dipole moments. We discuss a new kind of stripe which appears as a domain wall of the antiferromagnetic (AF) order parameter with a fractional change of the phase of the AF order. For large $|t'/t|$ spirals can be stabilized under certain conditions in the overdoped regime which may explain the elastic incommensurate magnetic response recently observed in iron-codoped Bi2201 materials.

PACS numbers: 71.27.+a, 73.22.Gk, 75.10.Lp

I. INTRODUCTION

The investigation of Hubbard type models with regard to solutions exhibiting modulated magnetic order is to a large extent motivated by (in)elastic neutron scattering experiments on high-temperature superconductors (for an overview cf. Ref. 1). Especially in the underdoped regime many compounds show a pronounced low energy spin response which is peaked away from the antiferromagnetic wave-vector. For overdoped samples of lanthanum cuprates it has been shown² that these low energy incommensurate spin fluctuations vanish at the same concentration where superconductivity disappears thus suggesting a close relation between both phenomena.

There are basically three possibilities which can account for the observed incommensurate spin response. First, the system can be close to a magnetic instability which in a random-phase approximation based treatment would strongly enhance the magnetic susceptibility at the corresponding wave-vectors. Moreover, in case of a superconducting (SC) d-wave gap the depletion of low energy spectral weight induces quasi undamped low energy incommensurate spin excitations which merge at the antiferromagnetic wave-vector into the famous resonance peak.³⁻⁵ This scenario is very popular in optimally doped YBCO, since the experimentally observed energy of the resonance peak scales with the SC transition temperature T_c as expected for this model. However, one could also envisage a situation of real symmetry breaking in the spin channel where (in terms of the above counting) the second and third possibilities correspond to ordered phases in the transverse and longitudinal spin channel, respectively. Since the charge couples to the square of the magnetic order parameter one expects in the latter case also a concomitant charge modulation. In lanthanum cuprates (LCO), doped with Ba or codoped with Nd or Eu,⁶⁻⁸ the third scenario is now well established. In these compounds the spin response even becomes static and con-

comitant charge order appears, which first was evidenced through the coupling to the lattice⁶ but recently more directly through soft resonant x-ray scattering.^{9,10} The fact that the periodicity of the charge modulation is half that of the spin strongly suggests that these materials have a so called ‘striped ground state’, i.e. quasi one dimensional antiphase domain walls of the antiferromagnetic order host the doped charge carriers. A polarized neutron scattering study on $\text{La}_{1.48}\text{Nd}_{0.4}\text{Sr}_{0.12}\text{CuO}_4$ ¹¹ in fact suggests that the magnetic order is one-dimensionally modulated although some two-dimensional noncollinear structure¹² may not be excluded.

It is worth noting that stripe textures have been predicted as stable Hartree-Fock (HF) saddle points of the Hubbard model¹³⁻¹⁵ before they were found experimentally in cuprates (and nickelates). However, it was realized early on that one has to include correlations beyond HF in order to correctly describe the experimental data in lanthanum cuprates. In the past years two of us have performed detailed investigations within the Gutzwiller approximation (GA) supplemented with Gaussian fluctuations which allowed for the explanation of the doping dependent incommensurability and various transport properties^{16,17}, the optical conductivity¹⁸ and magnetic excitations^{19,20} on the basis of striped ground states.

Non codoped lanthanum cuprates show a low energy inelastic incommensurability with a doping dependence rather similar to that of the codoped compounds suggesting the existence of some form of fluctuating and (or) disordered stripe order. Moreover, below a doping $\delta = 0.055$ the magnetic response rotates from vertical (i.e. along the Cu-O bond direction) to diagonal, becoming static and one-dimensional with the associated modulation along the orthorhombic b^* -axis, also in agreement with the stripe picture. On the other hand, direct probes of charge order are more difficult to obtain, leaving some room for the existence of incommensurate magnetic structures without charge order such as spirals. Although there are good hints from local probes like NMR,

NQR^{21–24} and tunneling²⁵ that point to charge ordered states, it is worth examining the possibility that transverse spin (spiral) textures exist.

Even more controversial is the situation in YBCO, the second class of high- T_c compounds which have been intensively investigated by neutron scattering (NS) experiments.¹ Since in optimally doped YBCO the low energy incommensurate magnetic response shows up below T_c , one line of thought is that the signal corresponds to the dispersion of a bound exciton which is formed inside a d-wave superconducting gap.^{26–30} However, it should be noted that for underdoped YBCO the observation of an incommensurate (and even static) spin response also above T_c ^{31,32} raises questions about this interpretation. In any case, the lack of experimental evidence for charge modulation in YBCO (which if dynamic or disordered is of course hard to detect) makes it difficult to conclusively attribute the incommensurate magnetic response to stripes as in codoped LCO, though it has been successfully described within a model based on slowly fluctuating (or disordered) charge stripes.³³ Also the quantum oscillations found in underdoped YBCO³⁴ are compatible with a reconstruction of the Fermi surface due to stripe order.^{35,36}

Due to the lack of large single crystals other cuprate superconductors are less intensively studied by NS than the aforementioned compounds. However, a recent study has revealed elastic incommensurate magnetic peaks in an overdoped $\text{Bi}_{1.75}\text{Pb}_{0.35}\text{Sr}_{1.9}\text{CuO}_{6+z}$ sample [(Bi,Pb)2201] codoped with iron.³⁷ Within the error bars the doping $\delta \approx 0.23$ and the measured incommensurability $\varepsilon \approx 0.21$ seem to extend the relation $\varepsilon \approx \delta$ (which holds for underdoped lanthanum cuprates³⁸) to large doping without saturation at $\delta \approx 0.12$.

An alternative to stripes in order to account for the incommensurate spin response in cuprates is based on the formation of spirals. These textures are characterized by a homogeneous periodic and planar rotation of the Cu moments with no associated charge modulation. Thus at first glance spirals seem to be a promising candidate for those cuprates in which incommensurate magnetic fluctuations have been observed without charge fluctuations, and corresponding theories have been recently put forward in Refs. 39–41.

Within Hubbard-type models spiral solutions have been investigated on the basis of HF,^{42–44} slave-boson (or GA)^{42,43,45–47} and dynamical mean-field⁴⁸ calculations. The energies of stripes and spirals have been computed within HF⁴⁹ and slave-boson methods^{45,46} based on the Hubbard model. These latter investigations have found a strong influence of the ratio between next-nearest and nearest neighbor hopping t'/t on the respective stability of both textures. Here our starting point is similar, however, we show that the low doping phase separation instability of spirals can lead to the formation of nanoscale charge and spin inhomogeneities with sub-

stantial spin canting. Stripes and spirals should therefore be viewed only as limiting cases of these more complex spin and charge textures. We discuss our findings with regard to recent neutron scattering experiments on iron-codoped lanthanum⁵⁰ and bismuth³⁷ cuprate superconductors. The paper is organized as follows. In Sec. II we introduce the formalism and present our results in Sec. III. Discussion and conclusions are presented in Sec. IV.

II. FORMALISM

Our starting point is the one-band Hubbard model

$$H = \sum_{i,j,\sigma} t_{ij} c_{i,\sigma}^\dagger c_{j,\sigma} + U \sum_i n_{i,\uparrow} n_{i,\downarrow}, \quad (1)$$

where $c_{i,\sigma}$ ($c_{i,\sigma}^\dagger$) destroys (creates) an electron with spin σ at site i , and $n_{i,\sigma} = c_{i,\sigma}^\dagger c_{i,\sigma}$. U is the on-site Hubbard repulsion and t_{ij} denotes the hopping parameter between sites i and j . We restrict to hopping between nearest ($\sim t$) and next-nearest ($\sim t'$) neighbors. Our approach is based on the Gutzwiller variational wave function $|\Psi_g\rangle = P_g |SD\rangle$ where P_g is the Gutzwiller projector and $|SD\rangle$ a Slater determinant. For $|SD\rangle$ we use a state with arbitrary charge and spin order, including spin canting. We define the associated one-body density as $\rho_{ij}^{\sigma_1, \sigma_2} = \langle SD | \hat{c}_{j\sigma_2}^\dagger \hat{c}_{i\sigma_1} | SD \rangle$. The wave-function optimization problem leads to a generalized Gutzwiller approximation⁵¹ which on the saddle-point level is equivalent to the Kotliar-Ruckenstein slave-boson approach⁵². The derivation of the spin-rotational invariant Gutzwiller energy functional can be found in Ref. 53

$$E^{GA} = \sum_{i,j} t_{ij} \langle \Psi_{\mathbf{i}}^\dagger \mathbf{z}_i \mathbf{z}_j \Psi_{\mathbf{j}} \rangle + U \sum_i D_i. \quad (2)$$

Here we have defined the spinor operators

$$\Psi_{\mathbf{i}}^\dagger = (c_{i\uparrow}^\dagger, c_{i\downarrow}^\dagger) \quad \Psi_{\mathbf{i}} = \begin{pmatrix} c_{i\uparrow} \\ c_{i\downarrow} \end{pmatrix}$$

and the \mathbf{z} -matrix

$$\mathbf{z}_i = \begin{pmatrix} z_{i\uparrow} \cos^2 \frac{\varphi_i}{2} + z_{i\downarrow} \sin^2 \frac{\varphi_i}{2} & \frac{S_i^-}{2S_i^z} [z_{i\uparrow} - z_{i\downarrow}] \cos \varphi_i \\ \frac{S_i^+}{2S_i^z} [z_{i\uparrow} - z_{i\downarrow}] \cos \varphi_i & z_{i\uparrow} \sin^2 \frac{\varphi_i}{2} + z_{i\downarrow} \cos^2 \frac{\varphi_i}{2} \end{pmatrix}$$

$$\tan^2 \varphi_i = \frac{S_i^+ S_i^-}{(S_i^z)^2}.$$

and for clarity spin expectation values in the *Slater determinant* are denoted by $S_i^+ = \rho_{ii}^{\uparrow, \downarrow}$, $S_i^- = \rho_{ii}^{\downarrow, \uparrow}$, $S_i^z = (\rho_{ii}^{\uparrow, \uparrow} - \rho_{ii}^{\downarrow, \downarrow})/2$, and $\rho_{ii} = \rho_{ii}^{\uparrow, \uparrow} + \rho_{ii}^{\downarrow, \downarrow}$. In the limit of a vanishing rotation angle φ the \mathbf{z} -matrix becomes diagonal and the renormalization factors

$$z_{i\sigma} = \frac{\sqrt{(1 - \rho_i + D_i)(\frac{1}{2}\rho_i + \frac{S_i^z}{\cos(\varphi_i)} - D_i)} + \sqrt{D_i(\frac{1}{2}\rho_i - \frac{S_i^z}{\cos(\varphi_i)} - D_i)}}{\sqrt{(\frac{1}{2}\rho_i + \frac{S_i^z}{\cos(\varphi_i)})(1 - \frac{1}{2}\rho_i - \frac{S_i^z}{\cos(\varphi_i)})}}$$

reduce to those of the standard GA. Spiral solutions are then computed by minimizing E^{GA} with respect to a homogeneous rotation of spins with wave-vector \mathbf{Q}

$$\begin{aligned} S_i^x &= S_0 \cos(\mathbf{Q}\mathbf{R}_i) \\ S_i^y &= S_0 \sin(\mathbf{Q}\mathbf{R}_i). \end{aligned} \quad (3)$$

In the present paper we usually measure modulations with respect to AF order $\mathbf{Q}_{AF} = (\pi, \pi)$ (lattice constant $a = 1$) and set $\mathbf{Q} = \mathbf{Q}_{AF} - \mathbf{q}$. Stripe solutions are obtained by restricting the magnetization to the z direction resulting in a modulation of S_i^z with \mathbf{Q} and a simultaneous modulation of ρ_i with $2\mathbf{Q}$ similar to our previous work.^{54,55} However, we also consider stripes and other charge ordered states with spin canting in Sec. III B.

III. RESULTS

In order to fix the value for the onsite repulsion U we refer to a previous paper where we have shown that a time-dependent extension of the GA with $U/t = 8$ can accurately reproduce the magnon excitations of undoped LCO²⁰ as revealed by neutron scattering.⁵⁶ Since U/t should not vary among the cuprate materials we restrict to $U/t = 8$ but investigate the dependence on the next-nearest neighbor hopping t'/t which from LDA computations has been shown to specify the various high- T_c families.⁵⁷ Note that the results of Refs. 45,46 have been obtained with a significantly larger value of $U/t = 12$.

A. Spirals vs. stripe states

Fig. 1 shows the energy landscape for spiral solutions (hole doping measured from half-filling $\delta = 0.2$) for different values of t'/t . With increasing $|t'/t|$ one observes a shift of the minimum from the vertical ($q_x, 0$) and $(0, q_y)$ directions towards the diagonal. Thus in the parameter regime relevant for LCO compounds $|t'/t| \sim 0.1 \dots 0.2$ the incommensurate scattering direction for the corresponding doping is correctly reproduced.

We note that also for other dopings only vertical or diagonal spiral textures correspond to minima of the energy landscape in agreement with previous investigations.^{42,43,45-47} This can be easily understood from the nesting curves⁵⁸ which are also shown in Fig. 1 below the energy contours. Basically these are $\mathbf{q} = 2\mathbf{k}_F$ plots (\mathbf{k}_F being the Fermi momentum) of the paramagnetic system backfolded in the $0 \leq \mathbf{q}_{x,y} \leq \pi$ quadrant. As discussed in Ref. 58 the dominant instabilities occur for

those wave vectors which correspond to a crossing of two nesting curves ('double nesting'). These double nesting points determine the maximum susceptibilities and are always found to lie along high-symmetry directions. The change from vertical to diagonal spirals upon increasing t'/t can therefore be understood from the appearance of an additional 'antinodal' double nesting vector along the $(0, 0) \rightarrow (\pi, \pi)$ direction which starts to dominate over those along the $(\pi, \pi) \rightarrow (\pi, 0), (0, \pi)$ directions.

The spiral is a realization of the corresponding instabilities, but the wave-vectors of energy minima and double nesting in Fig. 1 do not exactly coincide, as may be seen by comparing the nesting curves with the contour maps in lower parts of Fig. 1a,b,c. The Stoner criterion gives the correct nesting vector at the instability threshold, but as U/t increases the optimal q can shift. From 1 it can be seen that for $U/t = 8$ the spiral minimum coincides with the nesting curve near $t'/t = -0.2$, but is closer to (further from) (π, π) for large (smaller) t'/t .

Fig. 2 compares the doping evolution of vertical and diagonal spiral wave-vectors, for $t'/t = -0.2$ and $t'/t = -0.4$, with the corresponding values for vertical stripes (cf. also Ref. 54,59). The incommensurability is defined in terms of the wave-vector \mathbf{q} of the dominant Fourier component of the magnetization as

$$\varepsilon = \frac{|\mathbf{Q}_{AF} - \mathbf{q}|}{2\pi}$$

For stripes we restrict to regular, periodic stripe ground states with integer d (in terms of the lattice constant) separation between the charge stripes which amounts to a magnetic periodicity $2d$ and an incommensurability,

$$\varepsilon = \frac{1}{2d}$$

which develops a staircase structure, Fig. 2. The steps occur at the crossing of the corresponding energy curves (cf. Fig. 3). It is also convenient to define the number of doped holes per unit length along the stripe $\nu = \delta d$ which is related to the incommensurability by

$$\varepsilon = \frac{\delta}{2\nu}. \quad (4)$$

Given a certain number of holes one can ask if it is more favorable to add them to a small number of stripes with a large stripe filling or in a large number of stripes with a small stripe filling. For widely separated stripes one can determine an optimum linear density ν_o from

the minimum of the energy per hole with respect to half-filling^{16,54}

$$e_h = \frac{E_{N_h} - E_{AF}}{N_h}. \quad (5)$$

Here E_{N_h} is the total energy of the system doped with N_h holes. We find it convenient to use e_h to characterize the competition among the different phases at all dopings.

Fig. 3 compares e_h for stripes and spirals as a function of doping for $t'/t = -0.2$ and $t'/t = -0.4$, respectively. For stripes the individual curves correspond to vertically oriented domain walls and are labeled by the charge periodicity d . The optimum filling for large d is given by $\nu_o = d\delta_o$ with δ_o corresponding to the doping at the curve minimum. Notice that ν_o becomes independent of d for large d and takes the value $\nu_o = 0.55(0.4)$ for $t'/t = -0.2(-0.4)$. The change of ν_o with t' is expected according to the results of Ref. 54.

A constant ν_o implies via Eq. (4) a linear relation between doping and incommensurability. In other words the optimum filling determines the slope in the famous Yamada plot.³⁸

Where does the linear relation breaks down? The charged core of the stripe has a characteristic width ξ so that when the charge periodicity d is larger than ξ there are negligible interstripe interactions and doping proceeds by increasing the number of stripes. Therefore the relation is linear for $d > \xi$. In this regime the value of e_h at the minimum is independent of doping.

For $d \lesssim \xi$ stripe overlap becomes important and doping proceeds by increasing the charge of stripes. From Fig. 2 we see that $\xi \sim 4(5)$ for $t'/t = -0.2(-0.4)$ which can be checked directly from the charge profile (see Ref. 54).

As mentioned above the incommensurability for stripes shows a staircase structure. For small doping ($d > \xi$), since interstripe interactions are negligible, one can produce a practically continuous curve by considering combinations of solutions with periodicity d and $d + 1$. This becomes very costly for $d \lesssim \xi$ which is consistent with the tendency of the incommensurability to develop a plateau at doping larger than $\nu_o\xi \sim 1/8$.

As remarked before,^{16,20,54} the linear relation for small doping and the plateau for large doping reproduce the doping dependence of the incommensurate low energy magnetic response of lanthanum cuprates as revealed by neutron scattering experiments³⁸ and reproduced in Fig. 2.

For spirals, a minimum of e_h at doping δ_s indicates that if the frustration due to the long-range Coulomb interaction is ignored⁶⁰, the system will lower its energy by phase separating in undoped regions and spiral regions of doping δ_s . Contrary to the stripes, for spirals one observes a continuous increase of $\varepsilon(\delta)$. Nevertheless, both phases show similar evolution of incommensurability with doping and indeed fairly similar values of $\varepsilon(\delta)$ up to $\delta \sim \nu_o\xi$.

For larger doping this agreement is lost due to the tendency of stripes to make wide plateaus. In fact, both spi-

als and stripes originate from the same magnetic instability, the doping dependence of which has been analyzed for cuprate parameters in Ref. 58. In particular, it is the plateau in the spin susceptibility close to $Q_{AF} = (\pi, \pi)$ (cf. Fig. 1 in Ref. 58) which drives the system unstable towards spiral or stripe order for sufficiently large on-site repulsion U/t . We will come back to this point in the next section when discussing recent elastic neutron scattering experiments on overdoped Fe-LSCO⁵⁰ where the resulting incommensurabilities are shown as solid circles in Fig. 2.

We proceed by comparing the doping dependence of the energy minima which determine the orientation and respective stability of spirals and stripes. It should be noted that at low doping diagonal stripes are almost accidentally degenerate with vertical stripes with a negligibly preference for diagonal textures.¹⁷ Therefore other mechanisms like long-range Coulomb interactions, multiband effects, and lattice distortions are decisive in determining the exact stripe state in the very underdoped regime. In the following we restrict for simplicity to vertical stripes. The envelope (dashed-dotted line) for this set of curves represents the doping evolution for the stripe minimum energy and determines the doping dependence of the incommensurability as shown in Fig. 2.

The energy minima of the spiral landscape (cf. Fig. 1) are also shown in Fig. 3 as solid and dashed lines for diagonal and vertical spirals, respectively. As anticipated from Fig. 1 the crossover from diagonal to vertical spirals shifts towards higher doping with increasing $|t'/t|$ and it is found that for $t'/t = -0.4$ diagonal solutions are lower in energy over practically the whole doping range. However, for both diagonal and vertical spirals e_h has a minimum at δ_s which means that for doping smaller than δ_s spiral ground states are unstable with respect to phase separation as mentioned above. The resulting energy of the phase separated solutions calculated from a Maxwell construction is shown as a thin horizontal solid line in Fig. 3.

Also shown in Fig. 3 (full circle) is the energy of a single hole which is self-trapped in a spin-polaronic state. Since the corresponding charge is localized within a five-site plaquette with small ferromagnetic polarization, e_h for a many-polaron state will be independent of doping up to the point where polaron-polaron interactions become noticeable. For $t'/t = -0.2$, both spirals and polarons are unstable with respect to the stripe phase, whereas (diagonal) spirals become the stable phase for larger $|t'/t|$, consistent with the results of Ref. 58.

B. Charge order states with spin canting

The above finding that low doping spirals are unstable towards phase separation does not require that macroscopic phase separation is the ground state. There could exist inhomogeneous solutions with even lower energy. One could envisage e.g. an elliptical spiral⁶¹ correspond-

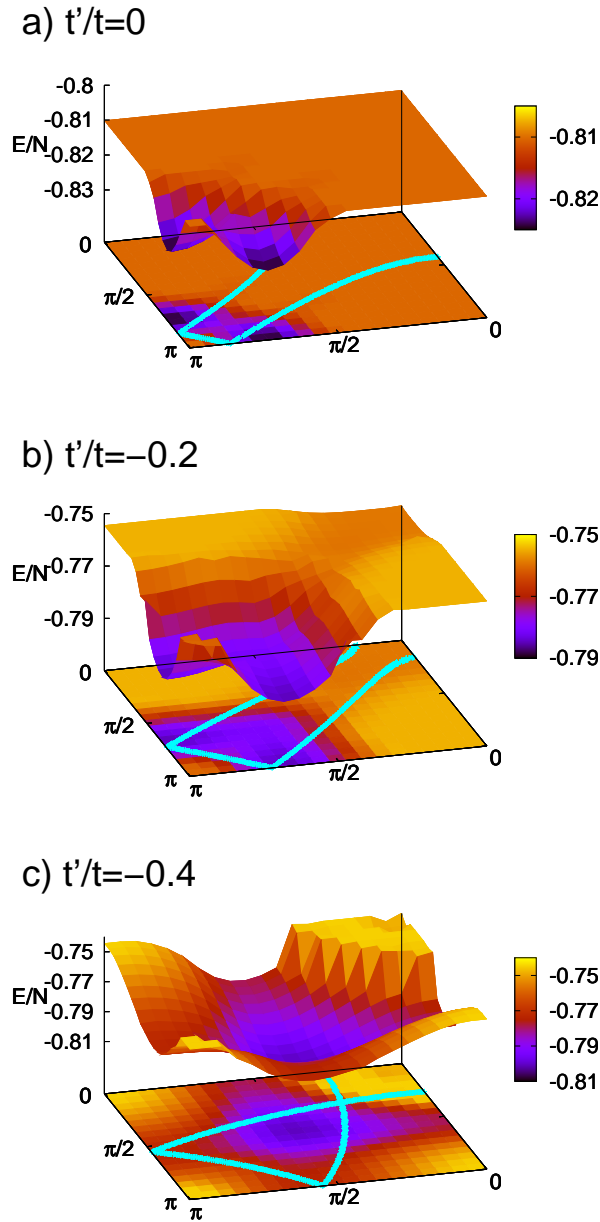


FIG. 1: (color online) Energy of spiral solutions (per lattice site and in units of t) as a function of spiral momentum $\mathbf{Q} = (q_x, q_y)$ (in units of the lattice constant $a \equiv 1$). Doping $\delta = 0.2$. The lines in the $(q_x, q_y, 0)$ -plane correspond to the nesting curves⁵⁸, obtained for the same doping in the paramagnetic state.

ing to spin structure

$$\begin{aligned} S_i^x &= S_0 \cos(\alpha) \cos(\mathbf{Q}\mathbf{R}_i) \\ S_i^y &= S_0 \sin(\alpha) \sin(\mathbf{Q}\mathbf{R}_i). \end{aligned} \quad (6)$$

which connects stripe and spiral states [cf. Eq. (3)] by tuning the eccentricity from $\alpha = 0$ to $\alpha = \pi/4$. As discussed below there are more complex structures which minimize the energy.

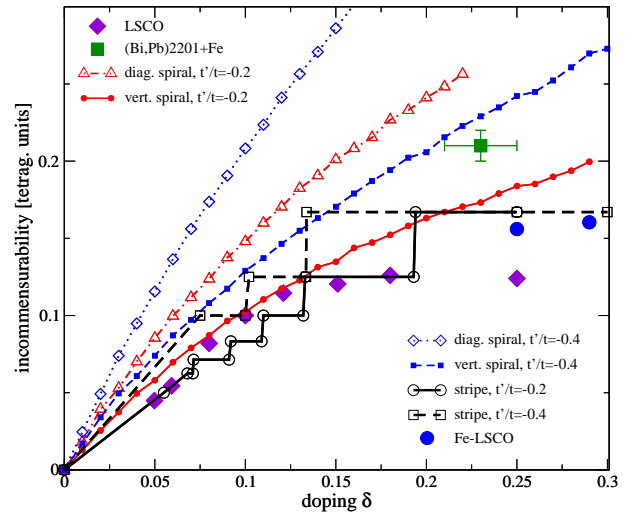


FIG. 2: (color online) Doping evolution of the spiral and stripe wave-vectors \mathbf{q} for $t'/t = -0.2$ and $t'/t = -0.4$ expressed in terms of the incommensurability. Note that the staircase structure of the stripe incommensurability is only explicitly shown for larger doping. The solid diamonds show the doping dependent incommensurability in LCO ('Yamada plot') and are reproduced from Ref. 38. The solid square corresponds to the elastic neutron scattering data on iron-codoped (Bi,Pb)2201 from Ref. 37. Solid circles report the incommensurability of Fe-LSCO from Ref. 50.

By performing an unconstrained minimization of the spin-rotational GA energy functional⁶² Eq. (2) on finite clusters, we find that for $t'/t = -0.4$ the low doping solutions are diagonal stripes with significant spin canting. An example is shown in Fig. 4(a) and the corresponding energy is indicated by the full square in Fig. 3(b). This texture is characterized by a domain wall of the antiferromagnetic order which has a fractional phase change of the AF order parameter $\Delta\theta < \pi$ (with θ the angle between the staggered magnetization and the quantization axis) contrary to collinear stripes which have $\Delta\theta = \pi$. Thus instead of building up a macroscopic phase separation between undoped AF and doped spiral regions (doping $\delta \approx 0.11$ as can be read from Fig. 3b), the system prefers to separate these textures at the nanoscale, corresponding to the modulated structure shown in Fig. 4(a). The material has clearly separated into ferromagnetically ordered diagonal lines which are at the center of 3-site wide spiral stripes with an average doping of $\delta \approx 0.11$ and undoped AF regions located between these stripes.

Research on multiferroics^{63,64} has shown that spin canting produces a force on the ligand ions via the Dzyaloshinskii-Moriya (DM) interaction⁶⁵⁻⁶⁸ which in some cases can lead to a uniform dipole moment. For the complicate textures we find the distortion is not uniform but can act as an experimental signature of the canted phases which we describe in some detail.

If we think of the one-band Hubbard model as embed-

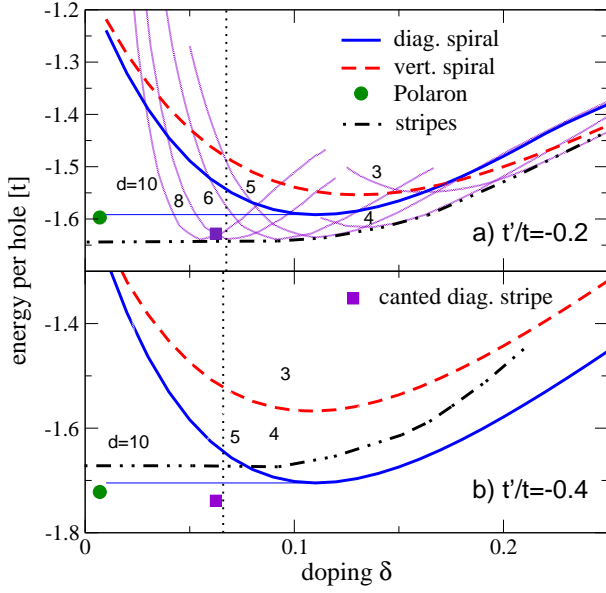


FIG. 3: (color online) Comparison of diagonal (blue solid) and vertical (red dashed) spirals with the energy of stripes (thin grey lines) for $t'/t = -0.2$ (a) and $t'/t = -0.4$ (b). The enveloping curve (dash-dotted) of the stripe energies is a guide to the eye. Vertical dotted lines indicate the concentration of zero compressibility for diagonal spirals and the thin solid line follows from the Maxwell construction. The full circle corresponds to the energy of a single spin polaron and the square is the energy of the spin-canted diagonal stripe which is shown in Fig. 4.

ded in the cuprate lattice, then the spin canting causes a force on the oxygen atoms, leading to a structural distortion of the CuO_2 planes. In the presence of spin-orbit interactions one can add to the Hamiltonian the following DM and elastic term:

$$H_{DM} = \sum_n \lambda \mathbf{u}_{n+1/2} \cdot \mathbf{f}_{n,n+1}^{DM}, \quad (7)$$

$$H_E = \sum_n \frac{k}{2} |\mathbf{u}_{n+1/2}|^2$$

where \mathbf{u} are the oxygen displacements and the DM force field is given by $\mathbf{f}_{ij}^{DM} \equiv \mathbf{e}_{i,j} \times \mathbf{S}_i \times \mathbf{S}_j$. Here $\mathbf{e}_{n,n+1}$ is a unit vector joining nearest neighbor Cu atoms. The product $\mathbf{S}_i \times \mathbf{S}_j$ is also known as the chiral vector order parameter.⁷⁰

For definiteness, we assume that the spins lie in the CuO_2 plane, as is approximately true for the cuprates. In this case, only the components of $\mathbf{S}_i \times \mathbf{S}_j$ perpendicular to this plane are finite, and \mathbf{f}_{ij}^{DM} lies in the plane at right angles to the Cu-O-Cu bond. Once \mathbf{f}_{ij}^{DM} becomes finite, $H_E + H_{DM}$ is minimized by developing a finite in-plane oxygen displacement perpendicular to the Cu-Cu bond. Due to the breaking of inversion symmetry around the oxygen atoms, this relaxation creates a local dipole moment.

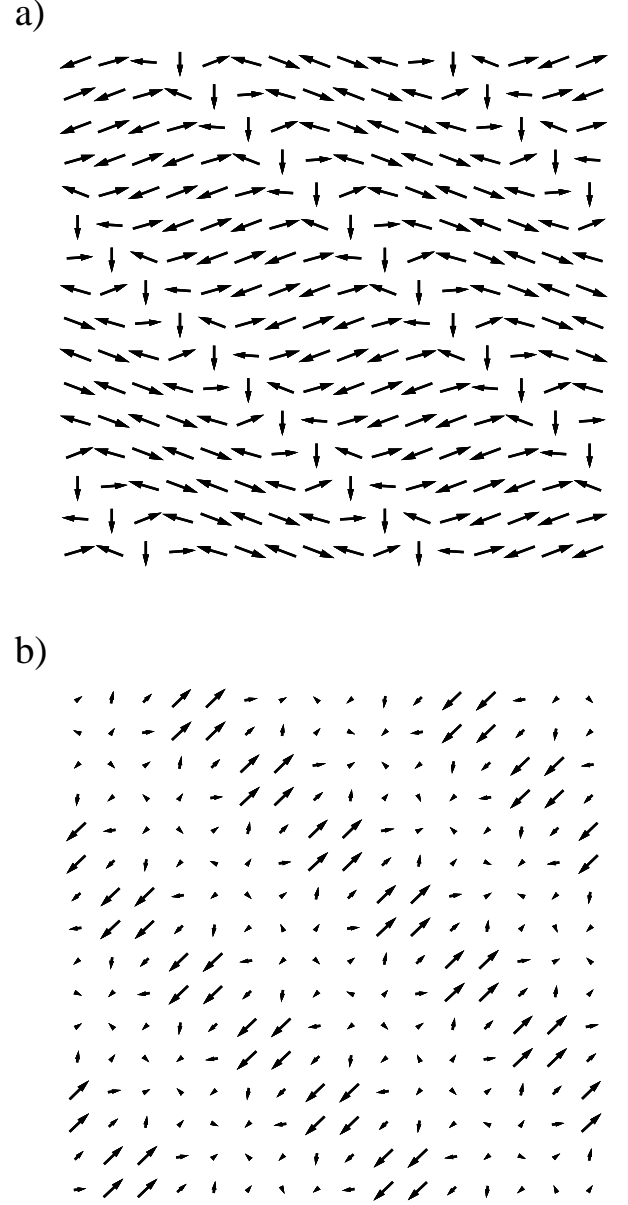


FIG. 4: a) Diagonal stripe solution with spin canting. The (hole) charge is accumulated on the lines with ferromagnetically aligned spins (parallel to the z -direction). b) Corresponding pattern of DM spin-currents \mathbf{j}_i^{DM} which are assigned to the lattice by summing the in- and outgoing currents of the connecting bonds, i.e. $\mathbf{j}_i^{DM} = \sum_j \mathbf{j}_{ij}^{DM}$. 16×16 system with 16 holes corresponding to doping $x = 1/16$. $U/t = 8$, $t'/t = -0.4$.

In the following we use the ‘DM current’ (or force flux)

$$\mathbf{j}_{ij}^{DM} \equiv |\mathbf{f}_{ij}^{DM}| \mathbf{e}_{i,j} = |\mathbf{S}_i \times \mathbf{S}_j| \mathbf{e}_{i,j} \quad (8)$$

in order to characterize the ground state magnetization pattern.^{71,72} These currents lie in the same plane as the spins and for the canted diagonal stripes are shown in

Fig. 4(b). One observes a maximal current perpendicular to the stripes with its direction alternating from stripe to stripe, so that the periodicity is the same as for the underlying spin structure. In contrast to the elliptic spirals, Eq. (6), which have a finite net force flux, the total spin force vanishes for our diagonal solution with an even number of stripes. The structure of the texture shown in Fig. 4 can be decomposed in harmonics as

$$\begin{aligned} S_i^x &= \sum_n S_n^x \cos(\mathbf{Q}^{(n)} \mathbf{R}_i) \\ S_i^y &= \sum_n S_n^y \cos(\mathbf{Q}^{(n)} \mathbf{R}_i) \end{aligned} \quad (9)$$

with $\mathbf{q} = (\frac{2\pi}{16}, \frac{2\pi}{16})$ and we have set $\mathbf{Q}^{(n)} = \mathbf{Q}_{AF} - n\mathbf{q}$. The solution breaks spin rotational symmetry, so the relative weights of the Fourier components on the x and y magnetization directions depend on the particular solution or quantization axis. For the choice shown in Fig. 4 the amplitudes are zero in the x (y) direction for n even (odd). The nonzero amplitudes are given by $S_1^x \approx 0.24$, $S_0^y \approx 0.03$, and $S_2^y \approx 0.1$. Therefore the x -component of the spin structure [Fig. 4(a)] induces incommensurate correlations at $\mathbf{Q} = (\pi - \frac{2\pi}{16}, \pi - \frac{2\pi}{16})$ and weaker ones at higher harmonics, $\mathbf{Q} = (\pi - \frac{4\pi}{16}, \pi - \frac{4\pi}{16})$, etc. In addition, the y -component leads to (weaker) commensurate correlations at $\mathbf{Q} = (\pi, \pi)$ and $\mathbf{Q} = (\pi - \frac{3\pi}{16}, \pi - \frac{3\pi}{16})$, etc.. Interestingly, this implies that in neutron scattering a weak commensurate peak will appear, a feature that may be hard to distinguish experimentally from phase separation between commensurate and incommensurate stripes.

For smaller values of $|t'/t|$, stripes do not profit from the transverse spin degrees of freedom and the energy of the spin canted solution is approximately that for the collinear solutions (cf. square symbol in Fig. 3(a)). Nevertheless, the finding that very different patterns are so close in energy suggests that stripes will be very susceptible to quenched disorder, inducing charge-spin glass behavior and making it difficult to obtain clear stripes signatures.

C. Checkerboard order for larger $|t'/t|$

In general, the spin canting allows the system to make a compromise between ferromagnetic order (which is favored for large $|t'/t|$ ^{73,74} and AF order induced by the local correlations. The fact that local ferromagnetism occurs for large values of the next-nearest neighbor hopping was also found to play a role in the stabilization of two-dimensional checkerboard textures with small ferron type clusters for large values of $t'/t = -0.5$.⁵⁹ These structures optimize the gain in kinetic energy for a collinear two-dimensional spin arrangement and turn out to be more stable than (collinear) stripes in this parameter regime. Based on our present findings it is thus natural to investigate the stability of spin-canted checkerboard textures.

Fig. 5(a) shows the minimum energy solution for 16 holes on a 16×16 lattice for $t'/t = -0.5$. Similar to our

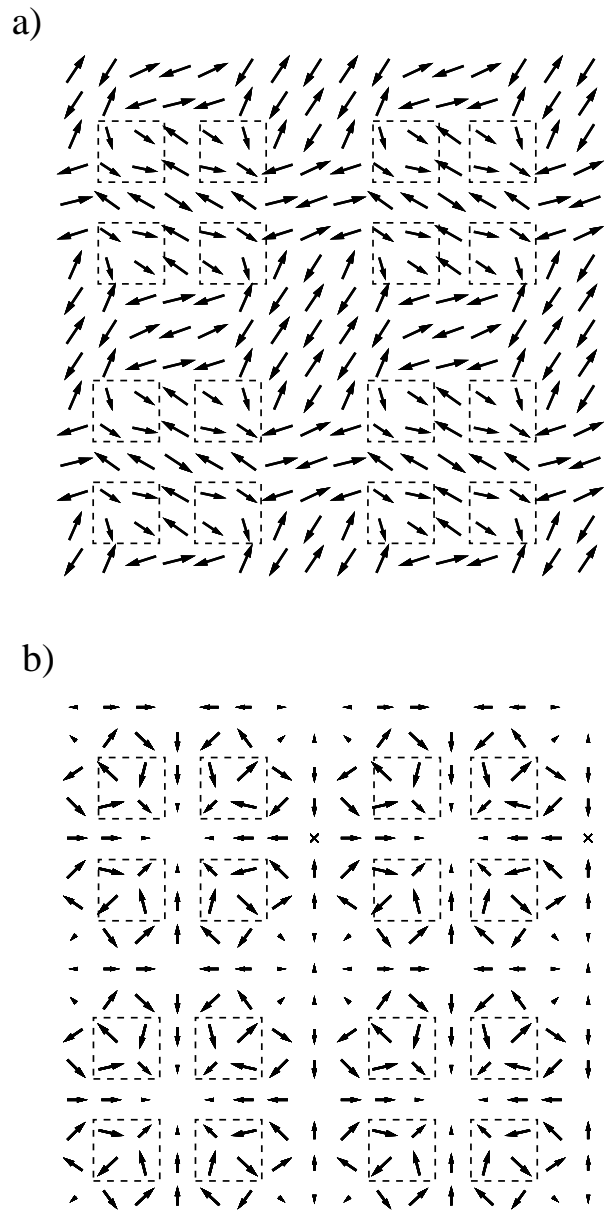


FIG. 5: Spin structure (a) and DM spin currents (b) for the two dimensional ‘checkerboard’ structure with spin canting. Regions with larger hole density are enclosed by boxes. 16×16 system with 16 holes corresponding to doping $x = 1/16$. $U/t = 8$, $t'/t = -0.5$.

previous findings in Ref. 59 it is only for such large values of t'/t that two-dimensional textures are stabilized over the (spin-canted) stripe solutions. The doped holes are confined to 2×2 plaquettes which are indicated by the dashed squares in Fig. 5(a). The overall pattern consists of a ‘checkerboard’ array of boxes each containing four charge plaquettes. The planar spin structure is no longer incommensurate but has dominant correlations at the AF wave-vector together with a finite ferromagnetic

moment. Again, the spin structure can be characterized by the associated ‘DM spin currents’ which are shown in Fig. 5(b). Here the centers of each box appear as a spin current sink whereas the center and corners of the lattice between boxes appear as sources for the spin current. Note that: 1) there is no net DM spin current as for a spiral so there will be no net dipole moment, 2) according to our definition the DM spin currents are useful to visualize the expected lattice distortions but do not correspond to currents of a conserved quantity.

We have also investigated the stability of vortex lattices which have been proposed by Fine¹² but found them always higher in energy than the checkerboard-type structures.

IV. DISCUSSION AND CONCLUSIONS

In a recent publication,⁵⁸ the magnetic phase diagram of cuprates was computed in terms of Fermi surface nesting, which determined the critical interactions U as a function of doping, and the leading incommensurate \mathbf{Q} vectors at threshold. The present calculations work at fixed U above threshold, but in general find very similar \mathbf{Q} values at fixed doping. Thus, for $t'/t = -0.4$, Fig. 3(b) shows a crossover from diagonal to vertical \mathbf{Q} as doping δ decreases. While Ref. 58 correctly predicted this *local* minimum, it missed the fact that the *global* minimum is determined by (nanoscale) phase separation. Similarly for $t'/t = -0.2$, the \mathbf{Q} of the vertical stripes is consistent with Fermi surface nesting⁵⁸ for $\delta \geq 1/8$, but not at lower doping.

Our investigations have revealed that the nature of symmetry-broken states in underdoped cuprates strongly depends on the strength of the next-nearest neighbor hopping. A value of t'/t , which is appropriate for lanthanum cuprates⁵⁷ stabilizes striped ground states so that the present analysis supports our related calculations on charge and magnetic excitations^{18–20} as well as transport properties¹⁶ in these compounds. Naturally the wave-function of such inhomogeneous textures is determined by states far from the Fermi energy so that one may question the present single-band analysis. However, we have checked by explicitly evaluating spirals and stripes within the three-band model that the conclusions of the present paper stay valid but the role of t'/t is played by the oxygen-oxygen hopping parameter.

In Fig. 2 we also show data from recent neutron scattering experiments⁵⁰ on Fe-LSCO. In these overdoped samples an elastic incommensurate spin response was found close to the dominant nesting vectors as extracted from ARPES experiments. It was thus concluded that the induced incommensurate response signals an inherent instability of the itinerant charge carriers, being different from the low doping stripes arising from localized Cu spins. Within our calculations (cf. Fig. 2) the data are rather close to the incommensurability curve of stripes obtained for $t'/t = -0.2$, which is the appropriate value

for LSCO.

Since our calculations are based on an itinerant approach, there is no ‘dichotomy’ between low doping ‘localized’ spin stripes and large doping itinerant ones, but both appear as different limits of the same model. In fact, at these large dopings one can also regard the stripes as arising from an instability of the ‘nearby’ (in energy) paramagnet similar to the spiral case as discussed in context to Fig. 1. In other words, increasing the doping one can go continuously from a stripe state at low doping to an itinerant spin-density wave (SDW) at high doping which disappears at a second order transition to become a uniform paramagnet.

At fixed doping one finds an analogous SDW instability with increasing U . For $t'/t = -0.2$ and $\delta = 0.3$ the spin density wave instability occurs at $\mathbf{Q} = (0.67\pi, \pi)$ and critical interaction $U_c/t \sim 2$. We can therefore view the $d = 3$ stripes (which have a similar periodicity) as the realization of this instability whereas spirals for these parameters have higher energy. Our GA calculations yield a charge modulation of only 8% for the $d = 3$ stripes at $\delta \sim 0.25$ which should be considered as an upper bound since our calculation neglects the effect of fluctuations. It may be therefore experimentally difficult to distinguish between a stripe and spiral state in this doping range.

For larger values of $|t'/t|$ as relevant for e.g. bismuthate high- T_c cuprates we have found that spiral textures are lower in energy than stripes in which canting is not allowed. If this latter restriction is relaxed, stripes and checkerboard states with a substantial spin canting become again more stable. This can be understood from the fact that spirals are unstable at low doping towards phase separation so that stripes and checkerboard states can be seen as nanoscale phase separated states.

It is interesting to remark that the more stable stripe at small doping is a novel kind of stripe with a fractional change in the phase of the order parameter as opposed to the usual π change. These states can be experimentally detected because they have a finite Bragg peak weight both at the commensurate AF wave vector $\mathbf{Q}_{AF} = \pi, \pi$ and at the incommensurate positions but can also be easily confused with phase separation among stripes and the commensurate antiferromagnet phase.

As shown in Figs. 4(b) and 5(b) the spin canting induces the flow of DM spin currents along the bonds of the lattice which are associated with the force flux \mathbf{f}_{ij}^{DM} . Due to the breaking of inversion symmetry arising from the oxygen displacements, such DM spin currents may be associated with an electric polarization $\mathbf{P} \sim \mathbf{f}_{ij}^{DM}$.⁷⁵

For the diagonal structure shown in Fig. 4(b), \mathbf{P} would point along the stripe but in alternate directions from stripe to stripe. On the other hand, in the nearly AF ordered regions between the domain walls the DM spin currents and thus the electric polarization almost vanish. The spin canted stripe can therefore also be considered as a one-dimensional ‘antiferroelectric’ with a vanishing net polarization.⁷⁶

In the overdoped regime and for sufficiently large $|t'/t|$

spirals do not phase separate and under certain conditions may constitute the ground state in cuprate superconductors. In this regard, the recent elastic NS study³⁷ on (Bi,Pb)2201 codoped with iron is interesting since it reveals incommensurate magnetic correlations with $\varepsilon \approx 0.21$ at a doping concentration $\delta \approx 0.23$. Our present computations shown in Fig. 2 suggest that the elastic neutron scattering data from Ref. 37 are compatible with vertical spirals provided that the value of the next-nearest hopping for Bi2201 is in the range $-0.4 < t'/t < -0.2$. LDA calculations by Pavarini and coworkers⁵⁷ yield a value of $t'/t \approx -0.25$ for Bi₂Sr₂CuO₆ where our results (cf. Fig. 3) suggest that vertical spirals are still more favorable than diagonal ones and may even dominate over stripes. Naturally, our computations which are for perfectly modulated spirals, can only be qualitative since the measured coherence length of the magnetic modulation³⁷ is of the order of the iron distance. Therefore additional effects like disorder and the magnetic moments arising from the Fe dopants should also be taken into account which is, however, beyond the scope of the present paper.

In the underdoped regime it is unlikely that uniform spirals will survive. Although for large $|t'/t|$ the phase separated spiral has nominally lower energy than the stripes, the macroscopically phase separated state implies a charge imbalance $\sim 0.1e$ per Cu which would result in

a prohibitive Coulomb cost.⁶⁰ Even without long-range Coulomb interaction a nanoscale phase separated state has lower energy.

Clearly the spin polarons, the checkerboard states as well as stripes, having charge inhomogeneities, will couple with impurities resulting in a spin and charge spin glass state consistent with experiments. Since this state will have substantial spin-canting it becomes rather semantic to distinguish it from the disordered spiral ground state as proposed by Sushkov.³⁹⁻⁴¹ For small $|t'/t|$ we expect that short-range diagonal stripes order dominates in this state as observed experimentally although with a correlation length of the static incommensurate response of the same order as the periodicity.⁷⁷ One should therefore rather think of a disordered state with meandering stripe which can profit from the impurity potential.

Acknowledgments

G.S. acknowledges financial support from the Deutsche Forschungsgemeinschaft. RSM's research is supported by the U.S.D.O.E contracts DE-FG02-07ER46352 and DE-AC03-76SF00098. J. Lorenzana's research is partially supported by the Italian Institute of Technology-Seed project NEWDFESCM.

-
- ¹ R. Birgeneau, C. Stock, J. M. Tranquada, and K. Yamada, *J. Phys. Soc. Jpn.* **75**, 111003 (2006).
² S. Wakimoto, H. Zhang, K. Yamada, I. Swainson, Hyunkyung Kim, and R. J. Birgeneau, *Phys. Rev. Lett.* **92**, 217004 (2004).
³ J. Rossat-Mignod, L.P. Regnault, C. Vettier, P. Bourges, P. Burlet, J. Bossy, J.Y. Henry, and G. Lapertot, *Physica C* **185-189**, 86 (1991).
⁴ H.A. Mook, M. Yethiraj, G. Aeppli, T.E. Mason, and T. Armstrong, *Phys. Rev. Lett.* **70**, 3490 (1993).
⁵ H.F. Fong, B. Keimer, P.W. Anderson, D. Reznik, F. Dogan, and I.A. Aksay, *Phys. Rev. Lett.* **75**, 316 (1995).
⁶ J. M. Tranquada, B. J. Sternlieb, J. D. Axe, Y. Nakamura, and S. Uchida, *Nature (London)* **375**, 561 (1995).
⁷ M. Fujita, H. Goka, K. Yamada, and M. Matsuda, *Phys. Rev. Lett.* **88**, 167008 (2002).
⁸ Klauss, H.-H. and Wagener, W. and Hillberg, M. and Kopmann, W. and Walf, H. and Litterst, F. J. and Hücker, M. and Büchner, B., *Phys. Rev. Lett.* **85**, 4590 (2000).
⁹ P. Abbamonte, A. Rusydi, S. Smadici, G. D. Gu, G. A. Sawatzky, and D. L. Feng, *Nature Phys.* **1**, 155 (2005).
¹⁰ J. Fink, E. Schierle, E. Weschke, J. Geck, D. Hawthorn, V. Soltwisch, H. Wadati and H.-H. Wu, *Phys. Rev. B* **79**, 100502 (2009).
¹¹ N.B. Christensen, H. M. Rønnow, J. Mesot, R. A. Ewings, N. Momono, M. Oda, M. Ido, M. Enderle, D. F. McMorrow, and A. T. Boothroyd, *Phys. Rev. Lett.* **98**, 197003 (2007).
¹² B. V. Fine, *Phys. Rev. B* **75**, 060504(R) (2007)
¹³ K. Machida, *Physica C* **158**, 192 (1989).
¹⁴ H. J. Schulz, *Phys. Rev. Lett.* **64**, 1445 (1990).
¹⁵ J. Zaanen and O. Gunnarsson, *Phys. Rev. B* **40**, 7391 (1989).
¹⁶ J. Lorenzana and G. Seibold, *Phys. Rev. Lett.* **89**, 136401 (2002).
¹⁷ G. Seibold and J. Lorenzana, *Phys. Rev. B* **80**, 012509 (2009); G. Seibold and J. Lorenzana, to appear in *Physica C*.
¹⁸ J. Lorenzana and G. Seibold, *Phys. Rev. Lett.* **90**, 66404 (2003).
¹⁹ G. Seibold and J. Lorenzana, *Phys. Rev. Lett.* **94**, 107006 (2005).
²⁰ G. Seibold and J. Lorenzana, *Phys. Rev. B* **73**, 144515 (2006).
²¹ S. Krämer and M. Mehring, *Phys. Rev. Lett.* **83**, 396 (1999).
²² P.M. Singer, A.W. Hunt, and T. Imai, *Phys. Rev. Lett.* **88**, 047602 (2002).
²³ J. Haase, C.P. Slichter, and C.T. Milling, *J. Supercond.* **15**, 339 (2002).
²⁴ D. Rybicki, J. Haase, M. Greven, G. Yu, Y. li, Y. cho, and X. Zhao, *J. Supercond. Nov. Magn.* **22**, 129 (2009).
²⁵ Y. Kohsaka, C. Taylor, K. Fujita, A. Schmidt, C. Lupien, T. Hanaguri, M. Azuma, M. Takano, H. Eisaki, H. Takagi, S. Uchida, and J. C. Davis, *Science* **315** (2007).
²⁶ M. Lavagna and G. Stemann, *Phys. Rev. B* **49**, 4235 (1994).
²⁷ D. Z. Liu, Y. Zha, and K. Levin, *Phys. Rev. Lett.* **75**, 4130 (1995).
²⁸ J. Brinckmann and P. A. Lee, *Phys. Rev. Lett.* **82**, 2915

- (1999).
- 29 M. R. Norman, Phys. Rev. B **61**, 14751 (2000).
 - 30 I. Eremin, D. K. Morr, A. V. Chubukov, K. Bennemann, and M. R. Norman, Phys. Rev. Lett. **94**, 147001 (2005).
 - 31 S. M. Hayden, H. A. Mook, P. Dai, T. G. Perring, and F. Dogan, Nature (London) **429**, 531 (2004).
 - 32 V. Hinkov, P. Bourges, S. Pailhès, Y. Sidis, A. Ivanov, C. D. Frost, T. G. Perring, C. T. Lin, D. P. Chen, and B. Keimer, Nature Physics **3**, 780 (2007).
 - 33 M. Vojta, T. Vojta, and R. K. Kaul, Phys. Rev. Lett. **97**, 097001 (2006).
 - 34 N. Doiron-Leyraud, C. Proust, D. LeBoeuf, J. Levallois, J.-B. Bonnemaïson, R. Liang, D. A. Bonn, W. N. Hardy, and Louis Taillefer, Nature **447**, 565 (2007).
 - 35 A. J. Millis and M. R. Norman, Phys. Rev. B **76**, 220503(R) (2007).
 - 36 S.E. Sebastian, N. Harrison, P.A. Goddard, M.M. Al-tarawneh, C.H. Mielke, R. Liang, D.A. Bonn, W.N. Hardy, O.K. Andersen, and G.G. Lonzarich, arXiv:1001.5015.
 - 37 H. Hiraka, Y. Hayashi, S. Wakimoto, M. Takeda, K. Kakurai, T. Adachi, Y. Koike, I. Yamada, M. Miyazaki, M. Hiraishi, S. Takeshita, A. Kohda, R. Kadono, J. M. Tranquada, and K. Yamada, arXiv:0907.3590.
 - 38 K. Yamada, C. H. Lee, K. Kurahashi, J. Wada, S. Wakimoto, S. Ueki, H. Kimura, Y. Endoh, S. Hosoya, G. Shirane, R. J. Birgeneau, M. Greven, M. A. Kastner, and Y. J. Kim, Phys. Rev. B **57**, 6165 (1998).
 - 39 O. P. Sushkov and V. N. Kotov, Phys. Rev. Lett. **94**, 097005 (2005).
 - 40 A. Lüscher, A. I. Milstein, and O. P. Sushkov, Phys. Rev. Lett. **98**, 037001 (2007).
 - 41 O. P. Sushkov, Phys. Rev. B **79**, 174519 (2009).
 - 42 E. Arrigoni and G. C. Strinati, Phys. Rev. B **44**, 7455 (1991).
 - 43 F. F. Assaad, Phys. Rev. B **47**, 7910 (1993).
 - 44 A. V. Chubukov and K. A. Musalian, Phys. Rev. B **51**, 12605 (1995).
 - 45 M. Raczkowski, R. Frésard, and A. M. Oleś, Europhysics Letters **76**, 128 (2006);
 - 46 M. Raczkowski, R. Frésard, and A. M. Oleś, Phys. Stat. Sol. (b) **244**, 2521 (2007).
 - 47 R. Frésard and P. Wölfle, J. Phys. Condens. Matter **4**, 3625 (1992).
 - 48 M. Fleck, A. I. Lichtenstein, A. M. Olés, and L. Hedin, Phys. Rev. B **60**, 1999.
 - 49 J. Zaanen and A. J. Olès, Ann. Physik **5**, 224 (1996).
 - 50 R.-H. He, M. Fujita, M. Enoki, M. Hashimoto, S. Iikubo, S.-K. Mo, H. Yao, T. Adachi, Y. Koike, Z. Hussain, Z.-X. Shen, and K. Yamada, arXiv:1009.1417.
 - 51 F. Gebhard, Phys. Rev. B **41**, 9452 (1990).
 - 52 G. Kotliar and A. E. Ruckenstein, Phys. Rev. Lett. **57**, 1362 (1986).
 - 53 J. Lorenzana and G. Seibold, Low Temp. Physics, **32**, 320 (2006).
 - 54 G. Seibold and J. Lorenzana, Phys. Rev. B **69**, 134513 (2004).
 - 55 R. S. Markiewicz, J. Lorenzana, and G. Seibold, Phys. Rev. B **81**, 014510 (2010).
 - 56 R. Coldea, S. M. Hayden, G. Aeppli, T. G. Perring, C. D. Frost, T. E. Mason, S.-W. Cheong, and Z. Fisk, Phys. Rev. Lett. **86**, 5377 (2001).
 - 57 E. Pavarini, I. Dasgupta, T. Saha-Dasgupta, O. Jepsen, and O.K. Andersen, Phys. Rev. Lett. **87**, 047003.
 - 58 R. S. Markiewicz, J. Lorenzana, G. Seibold, and A. Bansil, Phys. Rev. B **81**, 014509 (2010).
 - 59 G. Seibold, J. Lorenzana, and M. Grilli, Phys. Rev. B **75**, 100505(R) (2007).
 - 60 C. Ortix, J. Lorenzana, and C. Di Castro, Phys. Rev. B **73**, 245117 (2006).
 - 61 O. Zachar, S. A. Kivelson, and V. J. Emery, Phys. Rev. B **57**, 1422 (1998).
 - 62 G. Seibold, E. Sigmund, and V. Hiznyakov, Phys. Rev. B **57**, 6937 (1998); G. Seibold, Phys. Rev. B **58**, 15520 (1998).
 - 63 S. W. Cheong and M. Mostovoy, Nature Mat. **6**, 13 (2007).
 - 64 M.I. Katsnelson, Y.O. Kvashnin, V.V. Mazurenko, and A.I. Lichtenstein, Phys. Rev. B **82**, 100403 (2010).
 - 65 I. Dzyaloshinskii, J. Phys. Chem. Solids **4**, 241 (1958).
 - 66 T. Moriya, Phys. Rev. **120**, 91 (1960).
 - 67 D. Coffey, T.M. Rice, and F.C. Zhang, Phys. Rev. B **44**, 10112 (1991); N.E. Bonesteel, T.M. Rice, and F.C. Zhang, Phys. Rev. Lett. **68**, 2684 (1992); N.E. Bonesteel, Phys. Rev. B **47**, 11302 (1993).
 - 68 W. Koshibae, Y. Ohta, and S. Maekawa, Phys. Rev. B **47**, 3391 (1993);
 - 69 T. Yildirim, A.B. Harris, A. Aharony, and O. Entin-Wohlman, Phys. Rev. B **52**, 10239 (1995).
 - 70 S. Onoda and N. Nagaosa, Phys. Rev. Lett. **99**, 027206 (2007).
 - 71 Note that \mathbf{j}_{ij}^{DM} differs from the ground state spin current which describes the flow of the conserved magnetization and vanishes in our GA mean-field approach⁷².
 - 72 F. Schütz, P. Kopietz, and M. Kollar, Eur. Phys. J. B **41**, 557 (2004).
 - 73 T. Tohyama and S. Maekawa, Phys. Rev. B **49**, 3596 (1994).
 - 74 T. Hanisch, E. Müller-Hartmann, and G. S. Uhrig, Phys. Rev. B **56**, 13960 (1997).
 - 75 H. Katsura, N. Nagaosa, and A. V. Balatsky, Phys. Rev. Lett. **95**, 057205 (2005).
 - 76 The ‘antiferroelectric’ situation depends of course on the periodicity of the stripe structure. A different periodicity along (1, 1) may also result in a ferroelectric state.
 - 77 S. Wakimoto, R. J. Birgeneau, M. A. Kastner, Y. S. Lee, R. Erwin, P. M. Gehring, S. H. Lee, M. Fujita, Y. Yamada, Y. Endoh, K. Hirota, and G. Shirane, Phys. Rev. B **61**, 3699 (2000).